EUROPEAN ORGANIZATION FOR NUCLEAR RESEARCH

CERN/PS 89-35 (AR)

COPIOUS ELECTRON EMISSION FROM PLZT CERAMICS WITH A HIGH ZIRCONIUM CONCENTRATION

H. Gundel[1], J. Hańderek[2], H. Riege[1], E.J.N. Wilson[1] and K. Zioutas[3]

ABSTRACT

We describe the experimental method and report the results of electron emission from PLZT-2/95/5 ceramics subjected to rectangular HV pulses. The influence of HV amplitude, of gas pressure, and of temperature on electron beam current-density and charge was investigated. The kinetic energy was estimated by applying a decelerating field. Emitted current-density pulses of several A/cm^2 and charges of 1 μC/cm^2 are measured. A tentative interpretation is given.

(Submitted to Ferroelectrics)

---

1) CERN, CH-1211 Geneva 23, Switzerland.
2) University of Silesia, Institute of Physics, P-40007 Katowice, Poland.
3) University of Thessaloniki, Nuclear and Elementary Particle Physics Section, GR-54006, Thessaloniki, Greece.

1. INTRODUCTION

The emission of electrons from ferroelectric materials has been of interest for at least 30 years.[1] The materials investigated have included $BaTiO_3$[2-7] and other ferroelectric materials that are chemically similar.[1,8-23] The emission process has been studied when the crystals are placed in a vacuum chamber, in a gas at low pressure, and under atmospheric pressure. In this latter case, electrons are emitted accompanied by visible light. The emitted current density was at most 10^{-9} A/cm^2, and was much less in most cases.[3,24,25]

Let us imagine a static situation in which equilibrium has been reached between the spontaneous polarization P_s, the space-charge polarization $P_{sp.ch.}$, and the screening charges. If there is then a rapid change of P_s due to applying an electric field, mechanical pressure, or a temperature change, a large uncompensated surface charge $\pm\sigma$ will appear, owing to the difference in the time during which P_s changes and the Maxwellian relaxation time of the real surface charge. This uncompensated charge gives rise to a high electric field (10^5–10^7 V/cm) at the surface of the sample. If this surface is negative, then electrons that are drawn by this field from energy levels to which they are bound in the surface layer, will be accelerated. This process is described in detail by Rozenman et al.[23] on the basis of classical electrodynamics. The surface of an electron detector, placed above and parallel to the emitting surface of the crystal, may be thought of as a directing electrode. The negative charge, $-\sigma$, on the ferroelectric sample's surface is reflected in the detector's surface and appears as a positive charge, $+\sigma$, at an equal distance behind the plane of the detector. The authors of Ref. 23 report agreement between experiment and theory, based on this model, for electrons in the 5 to 100 keV energy range emitted from $LiTaO_3$.

A variety of procedures—thermal, optical, electrical, and mechanical, or their combinations—have been used to cause a rapid change in the components (P_s and $P_{sp.ch}$) of polarization. The electrons emitted have been recorded by electron channel multipliers, by Geiger-Müller-type counters (either in air at atmospheric pressure or in a stable gaseous environment), or by scintillation counters.

As far as we know, the emission of electrons from $Pb(Zr,Ti)O_3$ (PZT) and $(Pb,La)(Zr,Ti)O_3$ (PLZT) materials has not yet been investigated. Zirconium-rich PZT and PLZT solid solutions as well as pure $PbZrO_3$ have an antiferroelectric (AFE)–ferroelectric (FE)–paraelectric (PE) phase sequence, and the AFE–FE phase transition is strongly diffuse.[26-36] In crystals with separated defects of the oxygen and the lead sublattices, semiconductive properties also appear. This leads us to expect better conditions for the generation and emission of electrons.[37]

In this paper we present examples of experimental measurements of electron emission from PLZT-2/95/5 ceramic material generated by fast rising high-voltage and high-current pulses in a matched low-impedance circuit. The resulting emitted electron current and charge appear to be orders of magnitude higher than in the references mentioned above.

2. SPECIAL PROPERTIES OF PZT AND PLZT CERAMICS WITH HIGH ZIRCONIUM CONCENTRATION

At room-temperature and if the Ti content is 5%, the PZT and PLZT crystals are close to the nearly vertical FE–AFE boundary in the phase diagram of temperature versus composition.[26-31] This enables the AFE–FE transition to take place at a relatively low temperature.[26,28-30] We demonstrated that this occurs at about 50–60 °C in dielectric and pyroelectric investigations. Such measurements, and previous X-ray investigations on materials close to the AFE–FE phase boundary, have shown that the phase transition is strongly diffuse, and that the phases coexist in a broad band around the mean phase-transition temperature T_{A-F} between AFE and FE states.[32-35] The higher the Ti content is, the wider the band of temperature. Numerous sharp pyroelectric current pulses (Barkhausen pulses) are observed during AFE–FE transition through this band. When the sample is

pre-poled the number of metastable ferroelectric domains that remain in the antiferroelectric matrix is much larger. This is especially true of the surface layers. It was shown in Ref. 33 that below T_{A-F} the Barkhausen pulses are produced by pairs of ferroelectric domains with antiparallel P_s vectors which remain. The conditions that prevail in the vicinity of individual domains and individual grains influence the phase transition and especially the local transition temperature. The phase transition of the vast majority of the domains and grains in the bulk of the crystal will occur in the vicinity of T_{A-F}. However, surface layers of pre-poled ceramic samples have different electrical, and even chemical, properties. Moreover, differences in the internal electric field that supports P_s have an especially significant influence on phase transition in the surface. In Ref. 38 it was even shown that space-charge polarization of a polarized sample can shift the average T_{A-F} and T_{F-P} points, with T_{F-P} being the phase-transition temperature, between FE and PE states. We must therefore expect that compositional fluctuations near the morphotropy boundary of our sample of PLZT-2/95/5 ceramic material, as well as the separation of ion defects during the pre-poling, should cause differences in the local phase-transition temperature.

There is a separation of ionic defects into surface layers (mainly vacancies in the oxygen and lead sublattices) during preliminary polarization. This is called F-centre and V-centre absorption.[33,34] The space-charge polarization may be frozen in as a metastable state with very long relaxation time if the temperature is low enough. This may be achieved by pre-poling in the PE or FE phase and then cooling while maintaining the d.c. electric field. Oxygen vacancies with one or two electrons form F_1 and F_2 centres, respectively. The F_2 centres behave as donors, giving the surface layer n-type semiconducting properties. The conditions for electron generation from F_2 centres are drastically changed when the P_s vector is reversed.[23,24,34]

3. EXPERIMENTAL TECHNIQUE

Our investigations concentrated on a PLZT ceramic with composition 2/95/5. The three numbers refer to the La concentration and the ratio of Zr to Ti. The addition of La broadens the FE–AFE phase boundary and also lowers the electrical conductivity of the ceramic—two features which we judge have been crucial in achieving the high emission densities observed. Even more important are the semiconducting properties of the sample surface layers.

The disk-shaped samples were polished and covered with evaporated-gold electrodes, solid (SE) on one face and in the form of a grid (GE) on the opposite face (Fig. 1a).

Samples were pre-poled by applying a d.c. field of 2 kV/cm at 250 °C and cooling to room temperature over a period of about half an hour, while maintaining the field. The field was applied as a negative voltage to the GE face. Subsequently, electrical measurements of permittivity and resistance, and pyroelectric measurements were made to establish T_{A-F}. Because of the strongly diffuse AFE–FE phase transition, we can only give an approximate value for T_{A-F}.

Figure 1b shows a diagram of the experimental set-up. On the left we see the PLZT sample (FE) mounted in an electrically insulating support. The grid electrode GE is oriented towards the vacuum chamber. The insulation of the sample must be designed in such a way that rectangular high-voltage pulses may be applied without danger of breakdown across the sample edges. This part of the assembly is equipped with heater and thermocouple. The rest of the set-up is similar to the three-section analyser mentioned in Ref. 23.

The measuring electrode FC consists of a 3 mm thick perforated graphite disk, which communicates with the vacuum part on the right. The grid G_1 carries the positive image charge related to the negative surface charges on the sample surface. This can be considered as the source of the accelerating field.[23] Most of the measurements were carried out with G_1 11 mm from the sample surface GE. The grid G_1 also partly helps to eliminate noise originating from HV circuit components, piezo-vibrations of the sample and from other sources. The second of these grids, G_2, may be used to

apply a decelerating voltage without disturbing the acceleration due to the field between the sample and G_1. In this way, the energy of electrons passing through G_1 can be measured.

Some measurements were also made without using G_2 to apply voltages, and in this case the two grids were grounded or used as measuring electrodes such as FC. The transparency of the grids must always be taken into account and in order to determine it a negative high-voltage pulse was applied to the solid electrode, SE, of the sample with GE connected to ground. From the ratio of the integrated currents drawn by G_2 and FC it was possible to establish the transparency as 25%. The transparency of the mechanically identical grid G_1 is assumed to be the same.

Figure 1c shows the fast high-voltage pulse circuit with a 50 Ω impedance and a rise-time of 10 ns into a 50 Ω matching resistor. The maximum flat-top current delivered at 7.5 kV charging voltage is 75 A. Typical amplitude jitter of the HV pulse was better than 1%.

Figure 1d shows the measuring circuit. Emitted electrons that are collected by the two grids G_1 and G_2, and by the measuring electrode, FC, passed through a 50 Ω resistor. The current can be calculated from the voltage signal displayed on an oscilloscope connected across the resistor. An integrator with a capacitance of 21.5 nF and of 1 μs charging time was used to measure the total collected charge. The current pulses were measured on the oscilloscope with a 20 MHz bandwidth limitation in order to eliminate noise.

4. RESULTS

In the main series of measurements, the PLZT-2/95/5 sample was in a vacuum of 5×10^{-4} Pa. Figures 2a and 2b show the emitted charge (top), the emitted current (middle), both measured on FC with the circuits described above (see Fig. 1d), and the applied negative HV pulse (bottom) measured across the FE sample with an HV probe. Figures 2a and 2b show the waveforms for 30 kV/cm and 37.5 kV/cm electric field strength, respectively.

For 30 kV/cm (Fig. 2a) the electric field strength is below the threshold to initiate a P_s change. The FE sample behaves like a normal capacitor, and after filling this capacity the incoming rectangular pulse is matched by the 50 Ω resistor parallel to the FE sample (see Fig. 1c). The HV waveform thus shows a quasi-rectangular shape (Fig. 2a, bottom). Except for small induced oscillations (Fig. 2a, middle), no current signal is visible on the electrically independent measuring circuit connected to FC. Hence there is no net charge when being integrated (Fig. 2a, top).

In Fig. 2b the electrical field strength is high enough (37.5 kV/cm) to cause a P_s change. This distorts the HV waveform with positive peaks after the negative part (Fig. 2b, bottom). On FC the current was measured as shown in Fig. 2b (middle). The integrated waveform (Fig. 2b, top) shows the net charge, which decays with the rather short integration time, $t_{RC} = 1.08$ μs, of the measuring circuit. Thus the measured signal is not induced but represents, in fact, an emitted electron-beam current.

Electron current pulses are emitted at the beginning and at the end of the HV-pulse. A third electron pulse with much smaller amplitude may occur after a time corresponding to the HV pulse length, but always coinciding with a small positive peak in the HV waveform. Displayed on a faster time base (Fig. 3), the first pair of current peaks appear about 100 ns after the start of the applied HV pulse. When using the 20 MHz bandwidth limitation, each of the individual pulses is about 50 ns wide (FWHM). The next group of current pulses appears at the end of the HV pulse. Further pulses occur with diminishing strength. This complex structure is not fully understood but we discuss a possible explanation in Section 5.

There was considerable pulse-to-pulse scatter in the peak current and charge measurements, but this decreased as the applied voltage was increased. Typical amplitude jitter of current and charge measurement at an applied field of 37.5 kV/cm was ±20%. The experimental points used in Figs. 4–8 represent the average over 10 randomly chosen shots and the raw charge measurements

from the FC electrode are multiplied by a factor 50 to allow for the measured transparency of grids G_1 and G_2 and for the calculated area of the bare sample surface. The maximum value of the emitted electron current was 7 A/cm^2 for one single pulse and the maximum emitted charge was 1 μC/cm^2 for one component.

The purpose of the experiment was to establish how the number and strength of these current pulses depends on the applied voltage, the decelerating field, the gas pressure, and the temperature.

a. The influence of the applied electric field

We first investigated the field that is necessary in order to partially reverse P_s and to cause T_{A-F} to be shifted towards lower temperatures. Figure 4 shows the variation of the integrated current measurements as a function of applied field. The first and second charge components are plotted. The emitted charge density starts at a threshold of about 30 kV/cm and increases rapidly once the applied field reaches 35 kV/cm. Saturation was clearly not reached in these experiments, and even higher charge densities can be expected at higher applied fields. We restricted the maximum applied field to 37.5 kV/cm to guard against breakdown and possible perforation of the sample, and to ensure that the same one could be used for all measurements. The sample used for Fig. 4 had been pre-poled according to the prescription given above.

b. Determining the energy of the emitted electrons

The energy of the emitted electrons was determined by applying a negative potential to the grid G_2, and recording the current and charge reaching the FC electrode. Figure 5 shows the emitted charge density of the first component as a function of the decelerating negative potential of G_2. We show two sets of data for a field of a) 36 kV/cm and b) 37.5 kV/cm. The second and the third charge components disappear as the decelerating voltage rises from 0.2 to 0.5 kV, so at high enough decelerating voltage only the first charge step can be seen.

If we examine these curves closely, we see that the small increase in the decelerating voltage (0 to 0.2 kV) actually helps this first high-energy charge through, presumably by clearing the low-energy part of emitted components out of the way. We also see two linear regimes beyond this initial rise. In the first regime it seems as if one part of the electron spectrum below 1.7 keV is progressively excluded, whilst in the second regime a part below 3.8 keV is excluded. The lower curve shows similar behaviour in the case of 36 kV/cm. We were not able to make separate comparisons of the charge measurements for the individual current components at the beginning and end of the applied electric pulse, but current measurements of the two components (Fig. 6) suggest that they have similar energy distributions of electrons.

c. The influence of the air pressure

The results presented in subsections (a.) and (b.) were obtained in a vacuum of 5×10^{-4} Pa. In the next series of experiments we varied the pressure, measuring the emitted charge as above but with both G_1 and G_2 grounded. The curves of emitted charge density are shown in Fig. 7. Apart from the scatter in the data, it appears that the emitted charge density is approximately constant in the range from 10^{-4} to 10^{-1} Pa, whilst above 10^{-1} the emission begins to increase, probably because of charge multiplication.

d. The influence of temperature

The reversal of P_s and the shift of T_{A-F} under applied electric field pulses, as well as the electron states themselves in the surface layer of the sample, are temperature-dependent. This is especially true near the phase-transition point.[34] We have investigated the effect of temperature on the electron emission only in the region of diffused AFE–FE transition, where neighbouring AFE and FE phases

coexist.[35] Temperature dependence of emitted charge could be measured only approximately because the pre-poled state depends on temperature and time. This is particularly true at higher temperatures, where thermal electron generation from F-centres becomes more intense. The sample was heated continuously at a rate of about 1 K/min and the charge measurement was made at discrete temperature values. The results may be seen in Fig. 8. The tendency of the emitted charge increases with temperature and we expect this to become more pronounced close to the T_{F-P} phase-transition point.

5. DISCUSSION

Rozenman et al.[18,24] suggested, that electrons in the surface layer of a ferroelectric sample that appear because of unscreening during polarization change, can be emitted into the vacuum as a combined result of their self-field and of the tunnelling effect through the barrier of the potential trough. In two papers[15,23] these authors state that the electron emission can only take place from the negatively charged surface. Also in our experiments, where negative high-voltage pulses are applied to the solid electrode SE of the sample (Fig. 1a), uncompensated negative surface charges, $-\sigma$, appear on the bare part of the opposite sample surface, GE. The space-charge field arising from the charge density, $-\sigma$, accelerates the electrons towards the directing electrode, G_1. The final energy, to which the electrons are accelerated, is determined by the potential difference between the open surface of GE and G_1. Hence, the kinetic energy of the electrons and the emitted current density are determined by the surface charge density, $-\sigma$, and the distance between the electrodes GE and G_1.

In the case of PZT and PLZT ceramics with a high concentration of zirconium, the FE and AFE phases coexist in a broad band around their average T_{A-F} point. This fact, and the particular role of the F and V absorption centres which gives rise to space-charge polarization and to semiconducting n- and p-states in the surface layers, should be taken into consideration.

In the initial state of the pre-poled sample, F centres become concentrated in a thin layer on the sample surface, and the majority of them are filled by electrons forming F_2 centres (Fig. 9a). In this case the resultant space-charge polarization is near to zero but is still strong enough to have a resultant field supporting partial orientation of the remaining FE domains in the AFE matrix. This is sufficient to shift the T_{A-F} point,[34,38] especially in the surface layers of the sample.

Having applied the negative pulse to the solid electrode of the sample in order to reverse the spontaneous polarization, the negative ends of the existing FE domains terminate in the surface covered by the grid electrode. This applies equally to FE domains induced in the AFE matrix by the shift in the T_{A-F} point. In this situation the FE domains in the thin layer under the emitting surface of the sample play the most important role. The electrons, which previously played the role of screening these FE domains, can be emitted (Fig. 9). The electrons that are generated from the F_2 centres, $F_2^0 \rightarrow F_1^{1+} + 1e^-$ and $F_2^0 \rightarrow F_0^{2+} + 2e^-$, can also be emitted. All excess charges are repelled by the negatively charged bare surface of the sample caused by the induced ΔP_s. Another aspect is that the F_1^{1+} and F_0^{2+} centres lead to a partial compensation of P_s on this surface.

The first pulse of the first pair of current pulses emitted at the beginning of the HV pulse contains energetic electrons. The first probably stems from P_s reversal in the existing metastable ferroelectric domains (see Fig. 3). It is pointed out in Ref. 33 that below the T_{A-F} point they form twin domains with antiparallel P_s vectors. In this case, P_s reversal occurs only through the sideways displacement of the domain walls without the need for slower domain nucleation. The second current pulse in the group probably comes from nucleation of an FE domain formed in the AFE matrix as a result of the shift in the T_{A-F} point as the pulse is applied. The nuclei for this domain formation must be created before they can grow under the field by frontal and lateral domain boundary movement. Our hypothesis concerning these two current pulses is supported by the diagram of Fig. 6 where the energy of both electron pulses seems to be the same.

The subsequent groups of pulses in Fig. 2 appear at the end of the negative HV pulse on SE. The charge density and the energy of the individual pulses are weaker than those in the first group. Their appearance is linked to the positive-voltage peaks on SE. It seems that negative potential spikes occur simultaneously on the bare surface part of GE, which is the necessary condition for electron emission. The sample then returns to its initial state before the next HV pulse is applied. This concerns not only the state of P_s but also that of $P_{sp.ch.}$. The same is true for the F-centre states.

6. SUMMARY AND CONCLUSIONS

For the most favourable measurement conditions considered here (E_p = 37.5 kV/cm, p = 10^{-4} Pa, V_{g_2} in the range 200 to 500 V), shown in Figs. 5 and 6, the PZLT-2/95/5 ceramic sample emits the main group of energetic electrons, which appear 100 ns after switching on the applied pulse. Electrons flowing through the 50 Ω load resistor indicate a current density of several amperes per square centimetre. Previous workers[10,24] using different ferroelectric materials and experimental methods have found maximum emissions which are 10^9 or 10^{11} times weaker than this. The emitted charge measured by us is about 10^{-6} C/cm^2 (10^{13} electrons per cm^2). Provided the sample does not break down or is perforated first,[39] even higher charge densities can be expected before saturation occurs. A faster P_s change of the ferroelectric sample should also increase the emitted electron current density.

REFERENCES

1. A. Koller and M. Beranek, Czech. J. Phys. **9**, 402 (1959).
2. B. Sujak and J. Kusz, Acta Phys. Polon. **28**, 491 (1965).
3. V.S. Kortov and R.J. Mints, Fiz. Tverd. Tela **9**, 1828 (1967).
4. B. Sujak and J. Kusz, Acta Phys. Polon. **33**, 845 (1968).
5. B. Sujak and K. Biedrzycki, Acta Phys. Polon. **A42**, 49 (1972).
6. G.I. Rozenman, E.I. Boikova and Yu.L. Chepelev, Phys. Status Solidi (a) **69**, 173 (1982).
7. Yu.Ya. Tomashpolskii, E.I. Boikova, G.I. Rozenman and M.A. Sevestyakov, Fiz. Tverd. Tela **20**, 3491 (1978).
8. K. Biedrzycki, K. Sujak-Lesz and J. Lesz, Acta Phys. Polon. **A47**, 801 (1975).
9. B. Sujak and K. Biedrzycki, Proc. 5th Int. Symp. EEE and Dosimetry, Zvikov, 1976, p. 219.
10. P.F. Bräunlich, US Patent (1974).
11. B. Rosenblum, P. Bräunlich and I.P. Carrico, Appl. Phys. Lett. **25**, 17 (1974).
12. V.S. Kortov, K.K. Suvarts, A.F. Zatsepin, A.J. Gaprindashvily, A.V. Gulbis and Z.A. Grant, Fiz. Tverd. Tela **21**, 1897 (1979).
13. V.S. Kortov, A.F. Zatsepin, A.J. Gaprindashvily, M.M. Pinaeva, B.S. Vasilev and J.A. Morozov, Zh. Tekh. Fiz. **50**, 1934 (1980).
14. G.I. Rozenman and E.J. Boikova, Fiz. Tverd. Tela **21**, 1888 (1979).
15. G.I. Rozenman and E.J. Boikova, Phys. Status Solidi (a) **58**, 379 (1980).
16. G.I. Rozenman, J.R. Rez, Yu.L. Chepelev, N.B. Anhert and E.I. Boikova, Zh. Tekh. Fiz. **52** 1980 (1982).
17. G.I. Rozenman and V.I. Pechorskii, Fiz. Tverd. Tela **25**, 888 (1983).
18. G.I. Rozenman and V.I. Pechorskii, Yu.L. Chepelev, E.I. Boikova and L.E. Issakova, Phys. Status Solidi (b) **120**, 667 (1983).
19. G.I. Rozenman, I.S. Rez, Yu.L. Chepelev, N.B. Anhert and A.A. Zhashkov, Fiz. Tverd. Tela **22**, 3466 (1980).
20. G.I. Rozenman, I.S. Rez, Yu.L. Chepelev and N.B. Anhert, Zh. Tekh. Fiz. **51**, 404 (1981).
21. G.I. Rozenman, I.S. Rez, V.I. Pechorskii, Yu.L. Chepelev and N.B. Anhert, Zh. Tekh. Fiz. **51**, 1564 (1981).
22. E.I. Boikova and G.I. Rozenman, Fiz. Tverd. Tela **20**, 3425 (1978).
23. G.I. Rozenman, W.L. Bodiagin, Yu.L. Chepelev and L.I. Issakova, Radiotekh. and Elektron. **32**, 1997 (1987).
24. G.I. Rozenman, V.A. Okhapkin, Yu.L. Chepelev and V.Ya. Shur, Pis'ma Zh. Eksp. Teor. Fiz. **39**, 397 (1984).
25. L.M. Belaiev and G.G. Bendrikova, Fiz. Tverd. Tela **6**, 645 (1964).
26. J. Hańderek and Z. Ujma, Acta Phys. Polon. **A51**, 87 (1977).
27. J. Hańderek, Z. Ujma and K. Roleder, Phase Transitions **1**, 377 (1980).
28. K. Roleder and J. Hańderek, Phase Transitions **2**, 285 (1982).
29. Y.L. Wang, Z.M. Cheng, Y.R. Sun and X.H. Dai, Physica **B150**, 168 (1988).
30. M. Troccaz, Thèse, Lyon, No 1-75-005 (1975).
31. G.H. Heartling and C.E. Land, J. Am. Ceram. Soc. **54**, 1 (1971).
32. J. Hańderek, J. Kwapulinski, M. Pawełczyk and Z. Ujma, Phase Transitions **5**, 81 (1985).
33. J. Hańderek and K. Roleder, Ferroelectrics **67**, 159 (1987).
34. Z. Ujma and J. Hańderek, Phase Transitions **1**, 363 (1980).
35. J. Hańderek, J. Kwapulinski, Z. Ujma and K. Roleder, Ferroelectrics **81**, 253 (1988).
36. J. Hańderek, M. Pisarski and Z. Ujma, J. Phys. C **14**, 2007 (1981).

37. H. Gundel, H. Riege, E.J.N. Wilson, J. Hańderek and K. Zioutas, to be published in Nucl. Instrum. Methods (1989).
38. Z. Ujma and J. Hańderek, Ferroelectrics **33**, 37 (1981).
39. H. Gundel, H. Riege, E.J.N. Wilson, J. Hańderek and K. Zioutas, CERN PS/88-54(AR), paper presented at the First European Conf. on Applications of Polar Dielectrics and Int. Symp. on Applications of Ferroelectrics, Zurich, 1988 (Ferroelectrics, 1989).

FIGURE 1 The ferroelectric sample (FE) (a), experimental arrangement (b), the HV pulse circuit (c) and the measuring circuit for the emitted current and charge (d): FE - ferroelectric material; GE - grid electrode; SE - solid electrode; G_1, G_2 - auxiliary grids; FC - main measuring electrode; H - heater; T - thermocouple; S - HV switch.

FIGURE 2 The sample response to a negative rectangular pulse applied to the solid electrode SE of the FE (bottom, 25 kV/cm/div.), the emitted electron current (middle, 40 mA/div.), and the electron charge (top, 2.1 nC/div.) for an applied electric field strength a) $E_1 = 30$ kV/cm and b) $E_2 = 37.5$ kV/cm. Current and charge were measured on FC; the time scale is 500 ns/div. and the integration time is $t_{RC} = 1.08\ \mu s$.

FIGURE 3 Extended view of the emitted electron current pulse (top, 10 mA/small div.) measured on FC and the applied HV pulse (37.5 kV/cm) (bottom, 25 kV/cm/small div.). The signals were taken with a 20 MHz bandwidth limitation. The time scale is 100 ns/small div.

FIGURE 4 The electron charge density of the first two components as a function of the applied electric field-strength amplitude. The photo shows the three components of the integrated current (2.1 nC/div.) measured on FC (integration time $t_{RC} = 1.08\ \mu s$) for three different applied electric fields $E_1 = 35.25$ kV/cm (top), $E_2 = 36$ kV/cm (middle), and $E_3 = 37.5$ kV/cm (bottom). The time scale is 500 ns/div.

FIGURE 5 The emitted electron charge density of the first component versus decelerating voltage applied to the grid G_2 for $E_1 = 36$ kV/cm and $E_2 = 37.5$ kV/cm. The photo shows the three components of the integrated current (1.1 nC/small div.) measured on FC (integration time $t_{RC} = 1.08\ \mu s$) with an applied electric field $E = 37.5$ kV/cm for two different decelerating voltages $U_1 = 0$ V (upper trace) and $U_2 = -2000$ V (lower trace). The time scale is 200 ns/small div.

FIGURE 6 The maximum current density of pairs of electron pulses in the first (1a, 1b) and in the second (2a, 2b) component of the emitted charge as a function of the decelerating voltage on grid G_2 for an electric field-strength amplitude of 37.5 kV/cm. The photo shows the emitted current pulses (10 mA/small div.) measured on FC for two different decelerating voltages on G_2, $U_1 = 0$ V (upper trace) and $U_2 = -2000$ V (lower trace) with a time scale of 200 ns/small div. The signals were taken with a 20 MHz bandwidth limitation.

FIGURE 7 The dependence of the emitted electron charge density on air pressure for an electric field-strength amplitude of 37.5 kV/cm.

FIGURE 8 The temperature dependence of the emitted electron charge density for an electric field-strength amplitude of 37.5 kV/cm.

FIGURE 9 The semiconducting state of the pre-poled sample (a), the ferroelectric state after P_s reversal (b), and the coexistence of both states (c).

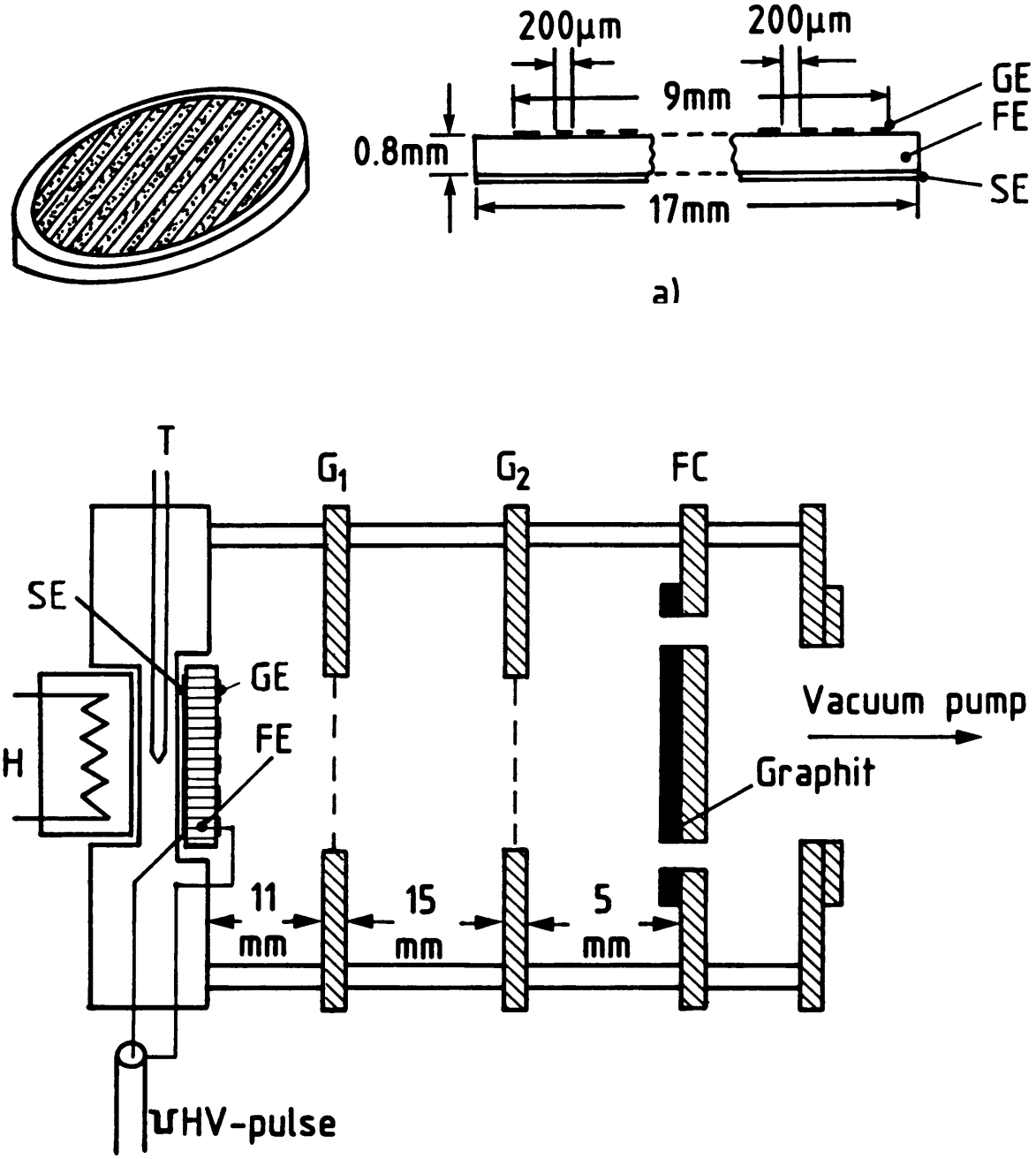
200µm
200µm
9mm
0.8mm
17mm
GE
FE
SE
a)
T
G1
G2
FC
SE
GE
FE
H
Vacuum pump
Graphit
11
mm
15
mm
5
mm
HV-pulse
b)

Fig. 1

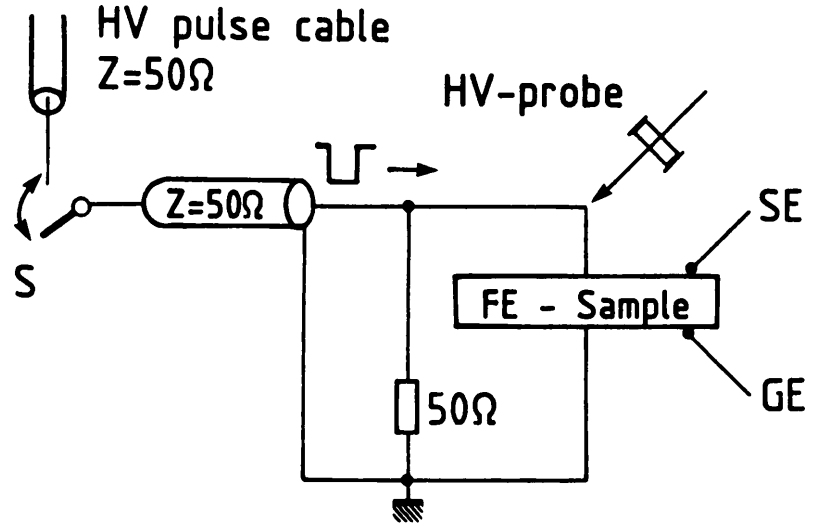
HV pulse cable
Z=50Ω
HV-probe
Z=50Ω
S
SE
FE - Sample
GE
50Ω

c)

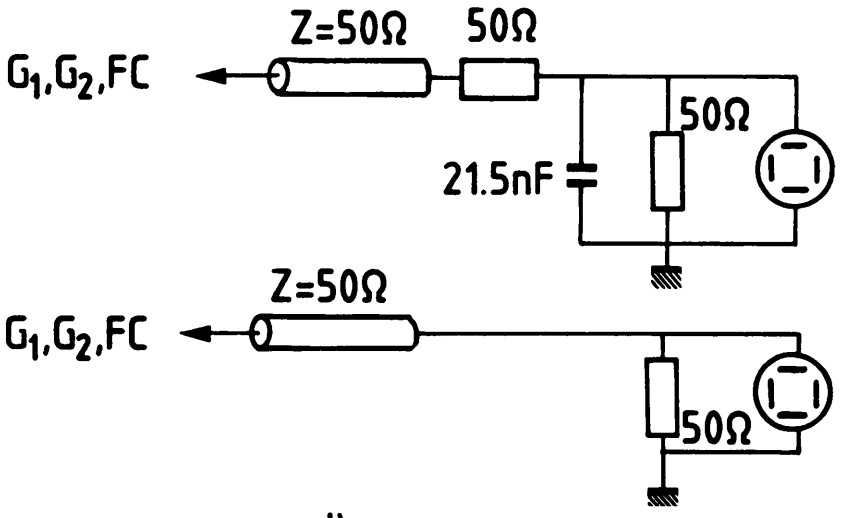
Z=50Ω
50Ω
G1,G2,FC
50Ω
21.5nF
Z=50Ω
G1,G2,FC
50Ω

d)

Fig. 1

a)

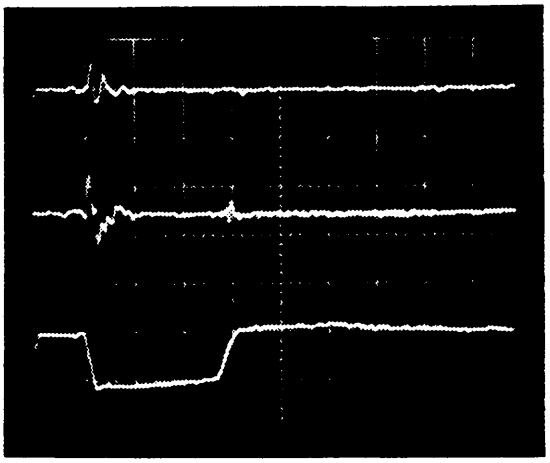

0.1 V/div.

2 V/div.

2 kV/div.

b)

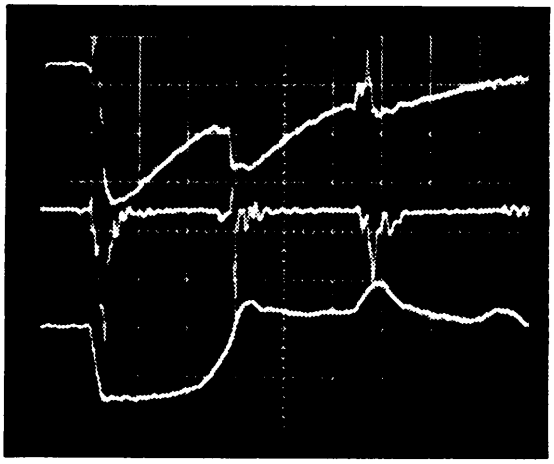

0.1 V/div.

2 V/div.

2 kV/div.

Fig. 2

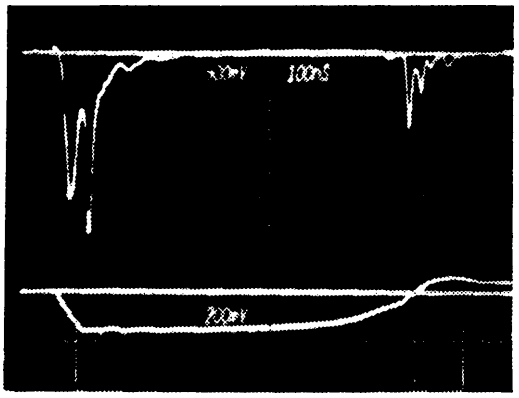

500 mV/small div.

2 kV/small div.

Fig. 3

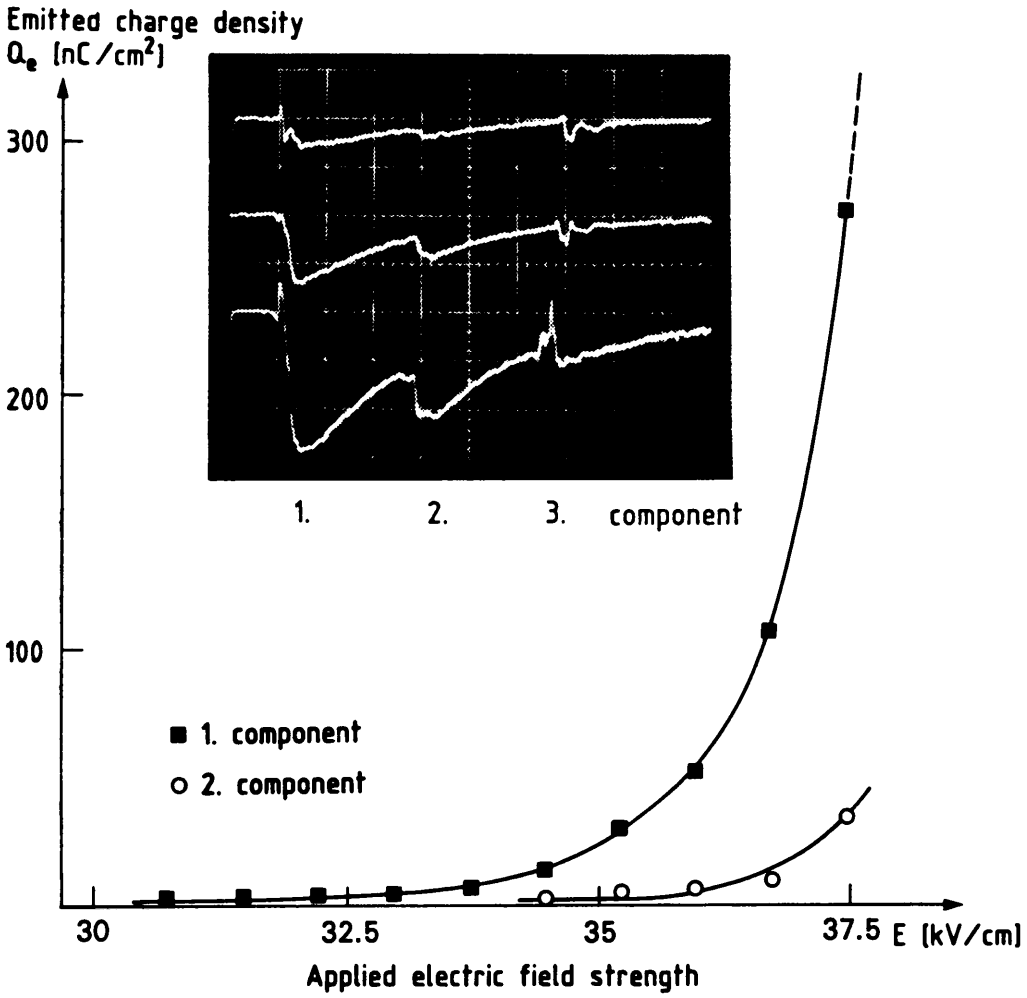
Emitted charge density
Q_e [nC/cm^2]
300
200
100
1. 2. 3. component
■ 1. component
○ 2. component
30
32.5
35
37.5 E [kV/cm]
Applied electric field strength

Fig. 4

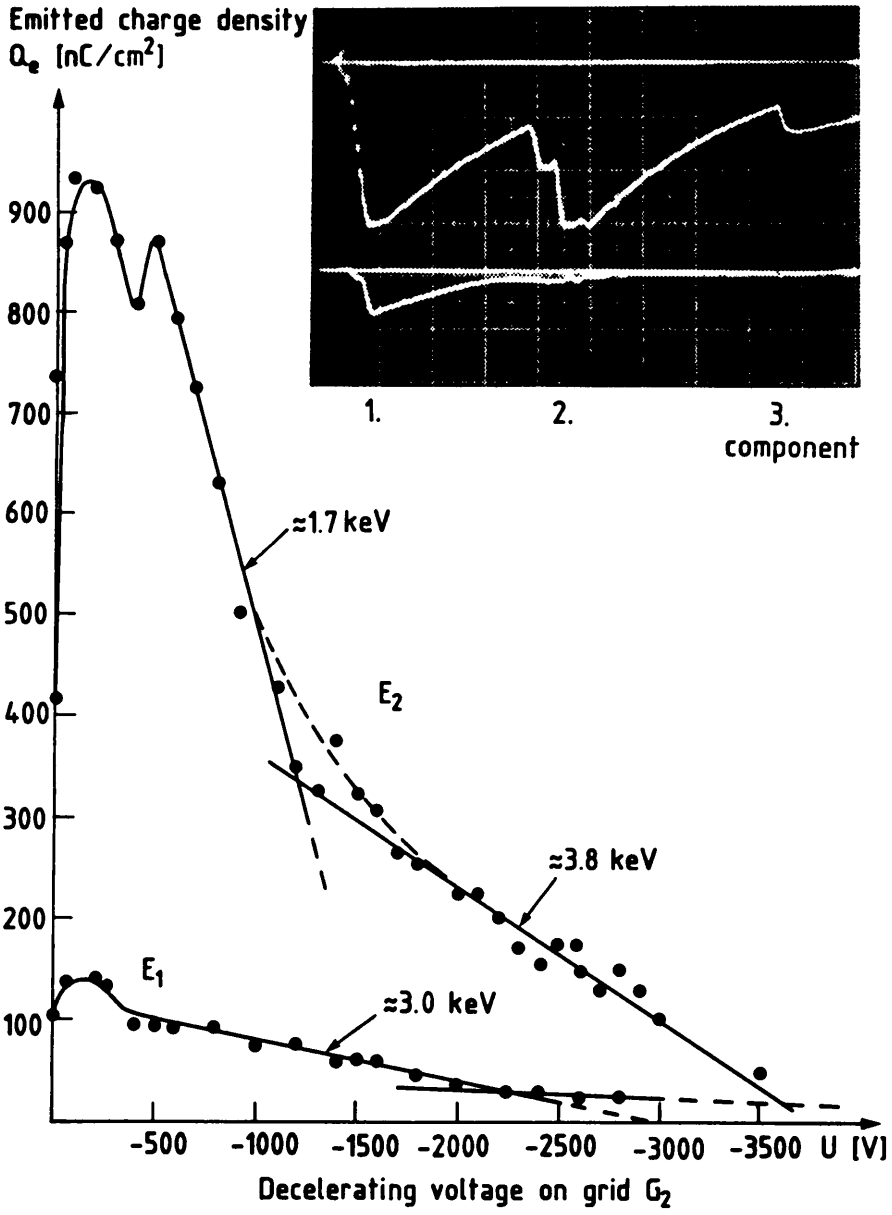
Emitted charge density
Q_e [nC/cm^2]
900
800
700
600
500
400
300
200
100
1.
2.
3.
component
≈1.7 keV
E_2
≈3.8 keV
E_1
≈3.0 keV
-500
-1000
-1500
-2000
-2500
-3000
-3500
U [V]
Decelerating voltage on grid G_2

Fig. 5

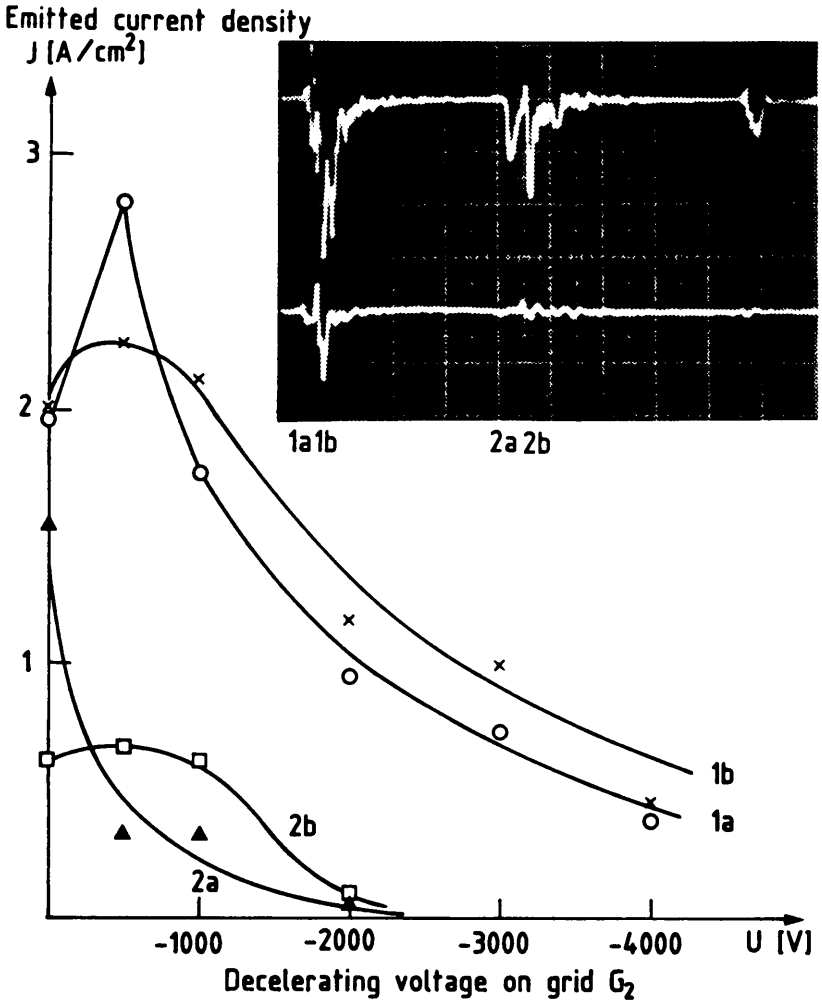
Emitted current density
J [A/cm²]
3
2
1
1a 1b
2a 2b
1b
1a
2b
2a
-1000
-2000
-3000
-4000
U [V]
Decelerating voltage on grid G2

Fig. 6

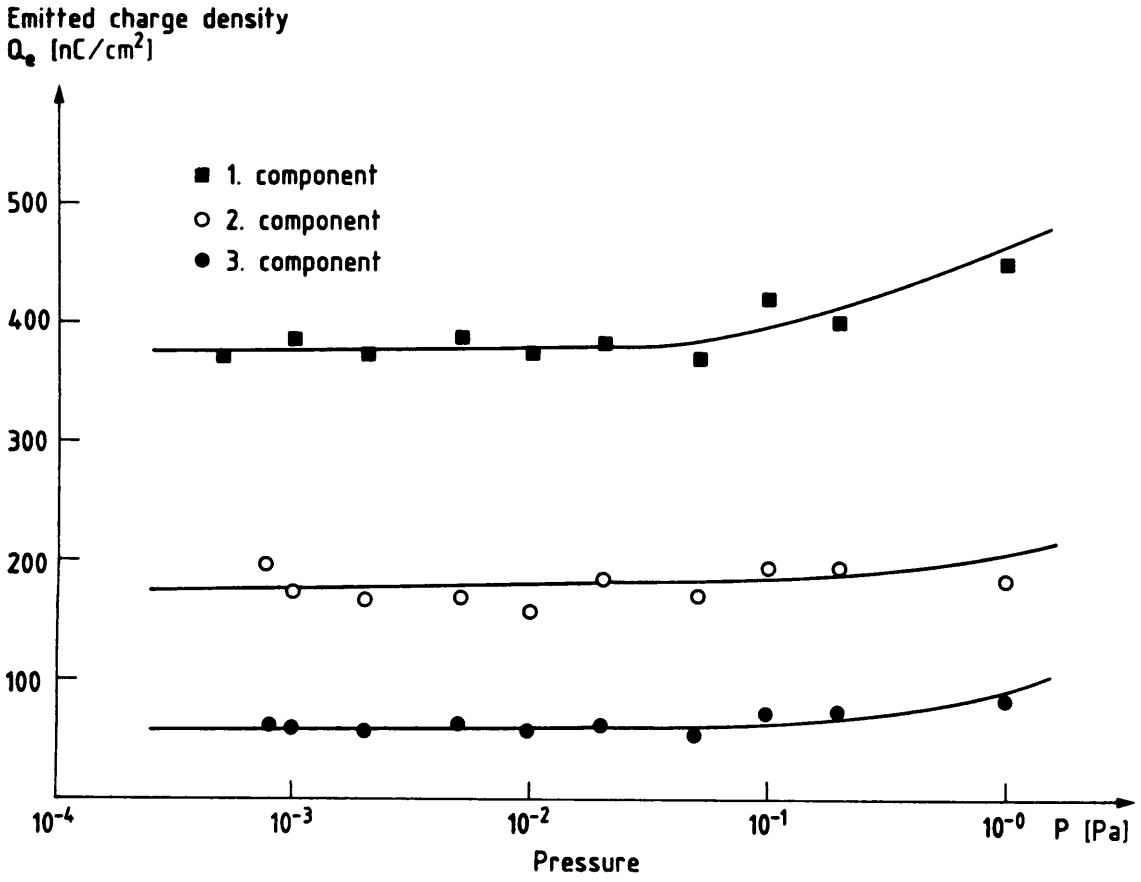
Emitted charge density
Q_e [nC/cm^2]
1. component
2. component
3. component
500
400
300
200
100
10^{-4}
10^{-3}
10^{-2}
10^{-1}
10^{-0}
P [Pa]
Pressure

Fig. 7

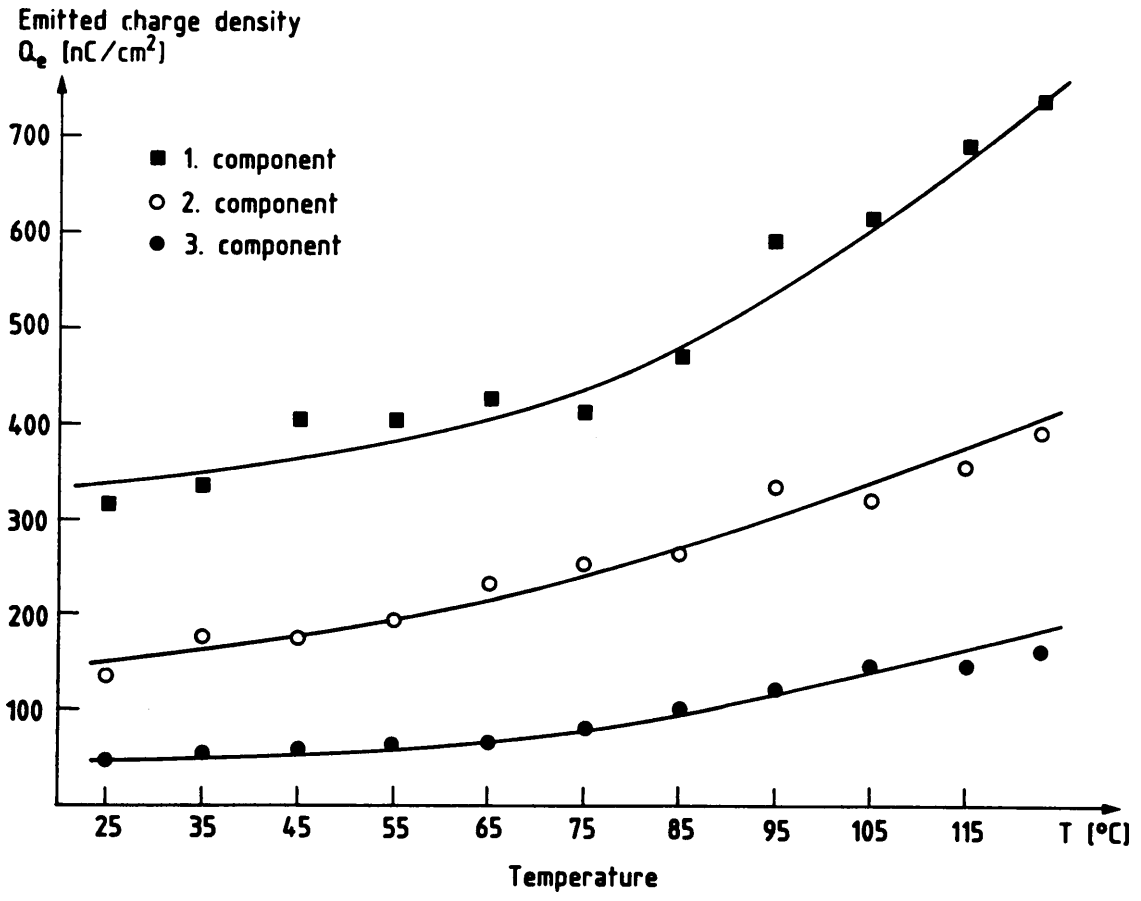
Emitted charge density
Q_e [nC/cm^2]
1. component
2. component
3. component
700
600
500
400
300
200
100
25
35
45
55
65
75
85
95
105
115
T [°C]
Temperature

Fig. 8

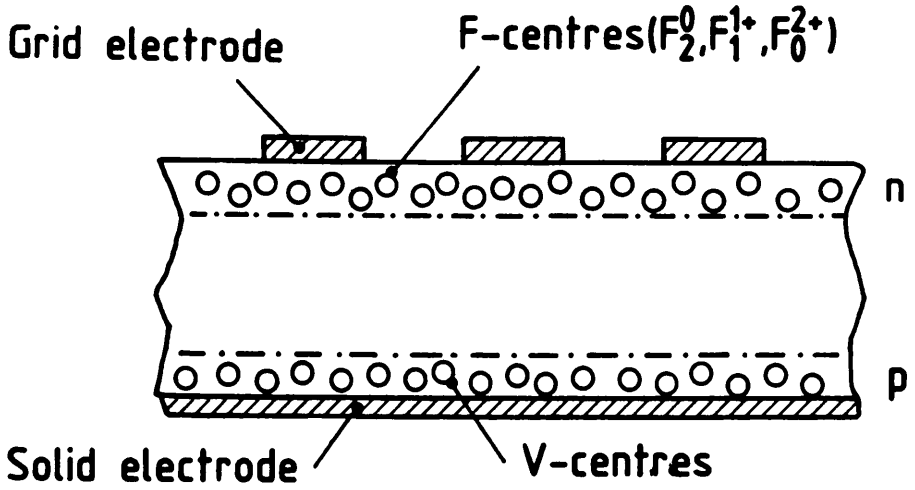
Grid electrode
F-centres(F_2^0,F_1^{1+},F_0^{2+})
n
p
Solid electrode
V-centres

a)

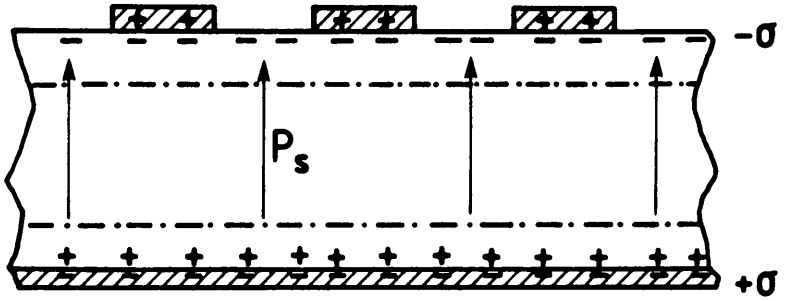
-σ
P_s
+σ

b)

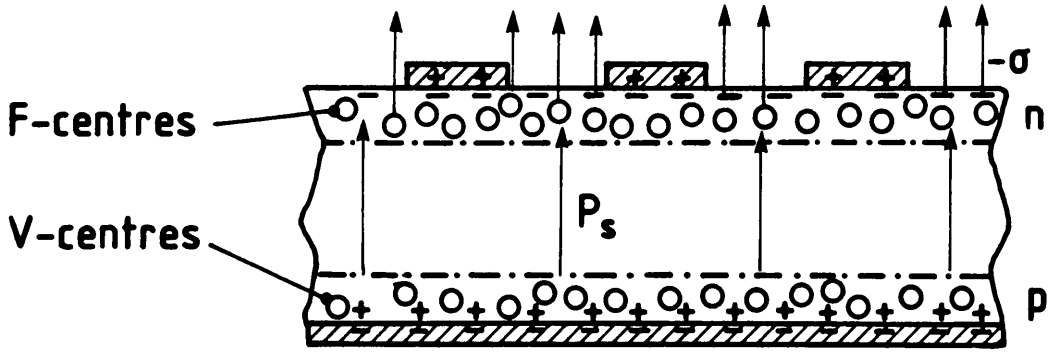
-σ
F-centres
n
P_s
V-centres
p

c)

Fig. 9